Flight Dynamics Prediction for Scaled Mars Rotorcraft

Allen Ruan
Aerospace Engineer
Analytical Mechanics Associates
NASA Ames Research Center
Moffett Field, CA, U.S.A.

Tove Ågren
Aerospace Engineer
Analytical Mechanics Associates
NASA Ames Research Center
Moffett Field, CA, U.S.A.

ABSTRACT

The use of sub-scale vehicles as a means of predicting full-scale vehicle behavior has historically been applied to flight dynamics testing and evaluation for aircraft operating in Earth atmospheric conditions. However, the use of sub-scale testing on Earth has not been as thoroughly explored for Martian rotorcraft. In this paper, sub-scale vehicles of varying sizes were developed in simulation using Froude scaling laws to evaluate their ability to estimate full-scale linear dynamics for the Mars hexacopter, Chopper. Blade loading, Lock number, and flap frequencies were held fixed when scaling and corresponding relationships for vehicle length, mass, inertia, and rotor speed derived. Full-scale frequency response, gain margin, and instability characteristics are explored for hover and forward flight cases in a variety of Mars-to-Mars and Earth-to-Mars conditions. Mach effects are also analyzed as a consequence of Froude-scaling by comparing sub-scale vehicles that are Mach-matched to the full-scale Chopper. Finally, a first-order approach for downselecting a sub-scale vehicle based on feasibility is introduced.

NOTATION

a	Speed of sound, m/s
A	Rotor disk area, m^2
C_{L_α}	Lift-curve slope
C_T	Rotor thrust coefficient, $T/(\rho A(\Omega R)^2)$
C_T/σ	Blade loading
c	Blade chord, m
Fr	Froude number, $V_{tip}^2/(gL)$
g	Gravity, m/s^2
G	Ratio of aerodynamic to vehicle inertia, $\rho C_{L_\alpha} N_b c R^2/(2m)$
EI	Blade flapwise bending stiffness
I	Moment of inertia, kgm^2
I_b	Blade inertia, $\int_0^R r^2 m dr$
L	Length, m
L,M,N	Stability/control derivatives for roll, pitch, yaw
m,M	Mass, kg
M_{tip}	Blade tip Mach number, V_{tip}/a
N	Length scaling factor, $N = L_f/L_s$
N_b	Number of blades
p,q,r	Body frame angular velocities
R	Rotor radius, m
Re	Chord-based Reynolds number, $\rho V c/\mu$
RPM	Rotor rotational speed, rev/min
T	Time, s
T	Thrust, N
u,v,w	Body frame translational velocities, m/s
V	Rotor speed at a given radial station, m/s
V_{tip}	Rotor tip speed, m/s
V_∞	Airspeed, m/s
X,Y,Z	Stability/control derivatives for longitudinal, lateral, and vertical translations
δ	Vehicle control input, %
γ	Lock number, $\rho C_{L_\alpha} c R^4/I_b$
μ	Advance ratio, $V_\infty \cos\theta/(\Omega R)$
μ	Dynamic viscosity, N·s/m^2
ν_β	Rotating natural flap frequency, rad/s
ρ	Density, kg/m^3
σ	Rotor solidity, $N_b c/(\pi R)$
ω	Frequency, rad/s or Hz
Ω	Rotor rotational speed, rad/s
ϕ,θ,ψ	Euler angles, rad

Subscripts

0.75	75% span
b	Blade
f	Full-scale
p	Lateral
q	Longitudinal
r	Yaw
s	Sub-scale
w	Heave

Presented at the Vertical Flight Society's 81st Annual Forum & Technology Display, Virginia Beach, VA, USA, May 20–22, 2025.

INTRODUCTION

Following the success of NASA's Ingenuity Mars Helicopter, next-generation Martian rotorcraft are being designed to fly

farther, faster, and carry out independent mission and science tasks. To provide sufficient power and maneuverability, proposed concepts, such as the Mars Science Helicopter (MSH) and Chopper, are planned to be substantially larger than Ingenuity's 1.8kg, 1.2m footprint; MSH is approximately 18kg, 3.9m while Chopper is approximately 33kg, 3.4m (Refs. 1, 2). As a result, experimental testing of the full vehicle will prove to be more challenging with space limitations in current low-pressure test facilities. In particular, using methods such as system identification (sys-id) (Ref. 3) to experimentally validate (linear) flight dynamics models of the full vehicle for control design may prove to be challenging in hover, and potentially infeasible in forward flight.

The flight dynamics model validation process for Ingenuity is documented in Ref. 4, where the bare airframe dynamics of Ingenuity were obtained through a "piece-wise" system identification campaign in which the vehicle was mounted in various configurations based on the derivatives being identified. Forward flight was imitated through the use of a wind wall and a swinging arm, in which the vehicle was affixed to the end of an arm of a test stand, which provided results of varying quality. Two years after Ingenuity landed on Mars, free flight system identification was then performed in flights 68 and 69 on the planet itself, concluding the validation process (Ref. 5). While these techniques were sufficient to validate Ingenuity's models, future missions can improve upon the model prediction and validation methods to be more accurate and generalized.

As new Mars rotorcraft grow in size, performing system identification on a fixed stand may prove challenging. However, free flight testing of the full-scale vehicle is not necessarily feasible either. Given space constraints in low-pressure testing facilities such as the 25ft. Space Simulator at NASA Jet Propulsion Laboratory (JPL) and the Planetary Aeolian Laboratory (PAL) at NASA Ames, free flight testing may be restricted to hover conditions. Forward flight tests would likely necessitate a sufficiently large wind tunnel, wind wall, or swinging arm apparatus.

Sub-scale testing may prove to be an intermediate means of predicting full-scale flight dynamics behavior as testing spaces are constrained, vehicle sizes grow, and opportunities to fly on Mars remain scarce. The use of sub-scale models for dynamic testing has been well documented in fixed wing (Refs. 6–8) and rotorcraft (Refs. 9–11), especially in the context of wind tunnel sub-scale testing. More recently, efforts to utilize smaller unmanned aerial systems (sUAS) to perform sub-scale flight tests for prediction of full-scale vehicle dynamics have been pursued by Mettler (Refs. 12–14) and Ivler (Refs. 15–17). However, while the vast majority of the existing literature focuses on Earth atmospheric conditions, examining the feasibility of scaling vehicles operating in Mars conditions is less explored. Scaling from Earth conditions to Mars conditions is nontrivial, as the difference in atmospheric density, speed of sound, and gravity, directly impacts the aerodynamic forces, moments, and damping experienced by the vehicle. Singh (Ref. 18) covers differences between the frequency response and open loop characteristics for the Mars Science Helicopter in Earth and Mars environments without scaling, noting the difficulties of designing and controlling a dynamically-matched surrogate helicopter.

This paper examines the design and analysis of Froude-scaled sub-scale vehicles as a means of predicting full-scale Mars rotorcraft linear dynamics through simulation. First, sub-scale vehicles of various lengths are compared to determine the predictive accuracy of Froude-scaling at a constant Martian density and gravity. Second, sub-scale vehicles are simulated in Earth gravity but Mars density to predict vehicle behavior in Mars gravity. Finally, models are simultaneously compared across various densities, gravitational accelerations, and length scales, with the ultimate goal of assessing if a sub-scale vehicle in Earth atmospheric density and gravity can be used to predict full-scale Mars vehicle behavior. The frequency response, as well as the full and reduced order linear time-invariant stability and control derivatives, for the sub-scale models are then scaled up to compare to those of the baseline full-scale model to validate the veracity of the scaling methodology and to study the effect of Mach number differences. The hover case is considered first, followed by forward flight conditions.

MODELING

Vehicle Characteristics

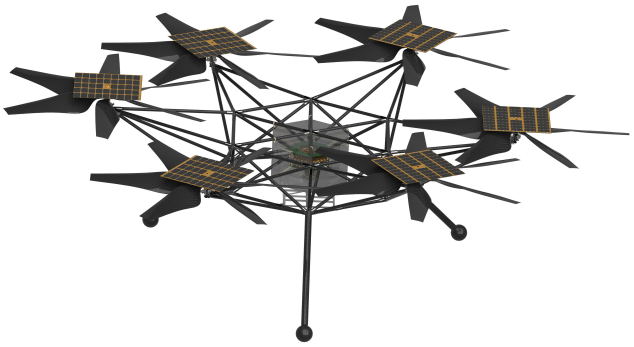

Figure 1. CAD rendering of the Chopper vehicle. Credit: NASA JPL.

The Chopper vehicle features six rotors, each containing 6 blades with an increased blade radius of 0.675 and a higher solidity of 0.3 compared to Ingenuity. For the current design iteration, the airfoils are very similar to the Ingenuity airfoils. Additionally, the rotor blades are designed to be sufficiently stiff, such that the rotor dynamics do not interfere with the rigid body dynamics in the frequency range of the controller. Details of Chopper's design methodology are covered in Ref. 2 and specific aspects of the blade design and wake modeling are covered in Refs. 19–21. The full vehicle is approximately 33kg and spans over 3.4m tip-to-tip. A full-scale model was developed in FLIGHTLAB, a finite element, multi-body, rotorcraft modeling and analysis tool (Ref. 22). The model consists of a rigid fuselage and six collective-controlled rotors with rigid blades. Flapping dynamics are modeled with

hinges, tuning hinge spring stiffness and damping to emulate the first physical flapping mode. A CAD rendering of the vehicle is shown in Fig. 1 and the corresponding FLIGHTLAB model is shown in Fig. 2.

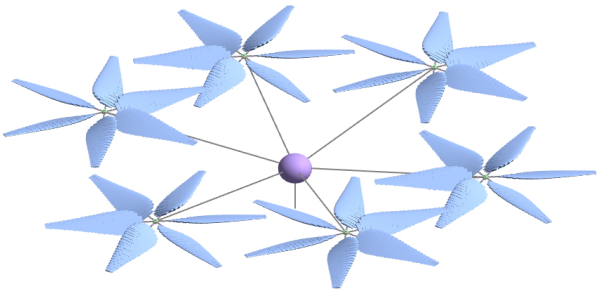

Figure 2. FLIGHTLAB model of the Chopper vehicle.

Rotor aerodynamic forces and moments are calculated using Blade Element Theory while the induced velocity is derived from a three-state Peters-He wake model detailed in Ref. 23. While rotor-rotor interactions are crucial to better understanding the complex aerodynamic effects of the multirotor configuration, they are not included in the modeling of this paper but are analyzed in Ref. 20.

Parametric Model

Robust control design and stability analysis is incumbent on obtaining sufficiently accurate mathematical models of the vehicle. Full and reduced order linear models are generated in FLIGHTLAB at a trim point using a perturbation method, which calculates partial derivatives of the residuals of generalized equations with respect to both states and inputs and are then averaged azimuthally.

The full order linear model for Chopper contains 108 states encapsulating rigid body, inflow, and flap dynamics. For control design, a quasi-static reduced order linear model can be obtained in the form $M\dot{x} = Fx + Gu$, where x is the state vector containing the rigid body states $x = [u; v; w; p; q; r; \phi; \theta; \psi]$ and u is the mixed input vector of directionally-aligned control inputs $u = [\delta_q; \delta_p; \delta_w; \delta_r]$. For body-frame dynamics, the sign convention is positive x forwards, positive y to the right, and positive z downwards. M denotes the diagonal mass matrix, containing vehicle mass and inertias. Assuming small vehicle trim angles, the corresponding stability and control derivative matrices are defined in Eq. (1) and Eq. (2), respectively.

$$F = \begin{bmatrix} X_u & X_v & X_w & X_p & X_q - w & X_r + v & 0 & -g & 0 \\ Y_u & Y_v & Y_w & Y_p + w & Y_q & Y_r - u & g & -g\theta\phi & 0 \\ Z_u & Z_v & Z_w & Z_p - v & Z_q + u & Z_r & -g\phi & -g\theta & 0 \\ L_u & L_v & L_w & L_p & L_q & L_r & L_\phi & L_\theta & L_\psi \\ M_u & M_v & M_w & M_p & M_q & M_r & M_\phi & M_\theta & M_\psi \\ N_u & N_v & N_w & N_p & N_q & N_r & N_\phi & N_\theta & N_\psi \\ 0 & 0 & 0 & 1 & \phi\theta & \theta & 0 & 0 & 0 \\ 0 & 0 & 0 & 0 & 1 & -\phi & 0 & 0 & 0 \\ 0 & 0 & 0 & 0 & \phi & 1 & 0 & 0 & 0 \end{bmatrix} \quad (1)$$

$$G = \begin{bmatrix} X_{\delta_q} & X_{\delta_p} & X_{\delta_w} & X_{\delta_r} \\ Y_{\delta_q} & Y_{\delta_p} & Y_{\delta_w} & Y_{\delta_r} \\ Z_{\delta_q} & Z_{\delta_p} & Z_{\delta_w} & Z_{\delta_r} \\ L_{\delta_q} & L_{\delta_p} & L_{\delta_w} & L_{\delta_r} \\ M_{\delta_q} & M_{\delta_p} & M_{\delta_w} & M_{\delta_r} \\ N_{\delta_q} & N_{\delta_p} & N_{\delta_w} & N_{\delta_r} \\ 0 & 0 & 0 & 0 \\ 0 & 0 & 0 & 0 \\ 0 & 0 & 0 & 0 \end{bmatrix} \quad (2)$$

Similar to most rotorcraft, Chopper is inherently unstable in open loop. For example, in hover, the longitudinal speed stability derivative (M_u), a derivative characterizing sensitivity to edgewise flow, governs the static stability of the vehicle and directly influences the frequency of unstable modes. The pitch damping derivative (M_q) also drives the magnitude of the instability, dominating over other terms such as the longitudinal speed damping (X_u). However, in forward flight, coupling of the lateral-longitudinal and vertical dynamics creates an increased sensitivity to pitch moments due to vertical speed perturbations, creating an angle of attack instability as a positive M_w. Given that this pitch-heave instability grows at higher advance ratios, it is of particular concern within control design and is explained in more detail in Ref. 24 and explicitly for Mars rotorcraft in Refs. 4, 25.

METHODOLOGY

Creating a representative sub-scale model stipulates that the ratio of the sub-scale vehicle's governing forces (i.e. aerodynamic, gravitational, and inertial) remain consistent with the full-scale's (Refs. 9, 14). Nondimensional parameters, such as the Froude, Mach, Reynolds, and Lock numbers, relate these forces such that vehicles of different sizes can be approximately compared. For example, matching the Froude number ensures the ratio of inertial to gravitational forces stays consistent between the sub-scale and full-scale vehicles. However, not all nondimensional terms can be adhered simultaneously (Ref. 26). For example, since both the Froude number and Reynolds number relate velocity to length scales independently, scaling with one would invariably violate the other. Within flight dynamics, scaling the vehicle based on a consistent Froude number has been extensively validated in literature and test programs, including, but not limited to, in Refs. 12, 13, 15, 27, and will be the primary means of scaling within this paper. Additional nondimensional parameters, such as the blade loading, are also scaled. The cumulative result is a methodology that simultaneously scales length components (e.g. rotor radius, hub-to-hub distance, chord), mass components (vehicle and blade mass), inertial components (vehicle and blade inertias), speed components (e.g. rotor rotational speed), and flapping components (e.g. hinge damping and stiffness).

Sub-scale Modeling

In the context of scaled modeling, N is conventionally used to represent the scale factor, defined in Eq. (3), as the ratio of the

characteristic length of the full-scale to the sub-scale vehicle. For example, if $N = 2$, the hub-to-hub distance of that sub-scale would be exactly 1/2 of the hub-to-hub distance of the full-scale vehicle.

$$L_s = \frac{1}{N} L_f \tag{3}$$

For a given length ratio and gravitational acceleration, Froude scaling establishes a scaling relationship for speed, length, and time parameters. Rotor speeds and forward flight speeds are Froude scaled such that simulations are compared at the same advance ratio (μ). Vehicle mass is then scaled based on density and length-scaling (and hence, volume). Done properly, the blade loading (C_T/σ) is thereby maintained to ensure each radial station is experiencing consistent lift. By extension, the rotor solidity of all sub-scale vehicles is maintained at 0.3, since both the chord and span of the blade are length-scaled. Lock number (γ) and G, a Lock number equivalent, defined in Ref. 24 as a representative ratio of aerodynamic to vehicle inertial forces, are used to scale the blade inertia and vehicle inertia, respectively. Finally, the flap stiffness is scaled to match the flap frequency. An overview of the scaling methodology can be found in Table 1, where L indicates a length unit, M indicates a mass unit, and T indicates a time unit. For example, to obtain a sub-scale vehicle's mass, the full-scale vehicle's mass is multiplied by the corresponding scale factor. Note that, while conventional tables in existing literature feature most Froude-scaled parameters solely as a function of the length-scaling factor N, Earth-to-Mars scaling must account for differences in gravity and density and are derived appropriately.

Table 1. Scale Factors for Key Vehicle Properties.

Property	Dimensions	Scale Factor	Matching
Length	L	$\frac{1}{N}$	-
Mass	M	$\frac{\rho_s}{\rho_f}\frac{1}{N^3}$	ρ, L
Frequency	$\frac{1}{T}$	$\sqrt{N}\sqrt{\frac{g_s}{g_f}}$	Fr
Velocity	$\frac{L}{T}$	$\frac{1}{\sqrt{N}}\sqrt{\frac{g_s}{g_f}}$	Fr
Inertia	ML^2	$\frac{\rho_s}{\rho_f}\frac{1}{N^5}$	γ, G
Stiffness	$\frac{ML^2}{T^2}$	$\frac{\rho_s}{\rho_f}\frac{g_s}{g_f}\frac{1}{N^4}$	ν_β

It is important to note that some of the simultaneous scaling laws presented may be practically infeasible. For example, maintaining the same C_T/σ in higher Earth densities increases the Earth sub-scale vehicle mass proportionally to the increase in atmospheric density. Similarly, matching flap response assuming the same material density for blades is highly intractable for a sub-scale vehicle and would potentially require using different material to maintain both the proper stiffness and density to satisfy both the flap frequency and Lock number matching. These feasibility concerns are explored at the end of the results.

Inevitably, Mach and Reynolds numbers will not remain constant across scales using this methodology. Mach number will vary since the rotor speeds are governed by Froude scaling, and if scaling from Earth to Mars, the speed of sound will differ. Taken together, the Mach number scales by $\frac{M_{tip,s}}{M_{tip,f}} = \frac{1}{\sqrt{N}}\sqrt{\frac{g_s}{g_f}}\frac{a_f}{a_s}$, decreasing at a rate of $\frac{1}{\sqrt{N}}$ as sub-scale sizes shrink in the same atmosphere and gravity. When comparing Mach from Earth to Mars for sub-scales close to the full-scale size, the difference in gravitational acceleration dominates, leading to a higher Mach than on Mars. Conversely, Earth sub-scales have a significantly lower Mach when the sub-scale size shrinks and speed of sound grows.

Similarly, Reynolds number can not be matched since Froude formally relates rotor speed and length scales, and for Earth-to-Mars scaling, the Reynolds number scales by $\frac{Re_s}{Re_f} = \frac{1}{N\sqrt{N}}\sqrt{\frac{g_s}{g_f}}\frac{\rho_s}{\rho_f}\frac{\mu_f}{\mu_s}$. At a constant density, gravity, and dynamic viscosity, the length difference of smaller vehicles (higher N) scales as a function of $N^{-3/2}$, decreasing Reynolds number dramatically when Froude scaling (an 1/8th-scale vehicle has a Reynold's number of $\approx 5\%$ the full-scale Chopper). For Earth-to-Mars scaling, the Reynolds number reduction is countered by the ratio of air densities, allowing for more similar Reynolds values for smaller vehicles at higher atmospheric densities on Earth and drastically higher Reynolds for larger vehicles.

However, given the simulation-based nature of this work, one can artificially match the Mach number of the full-scale vehicle by manipulating the speed of sound to offset the Mach reduction from length and speed scaling to assess the impact of Mach effects. Runs that adjust the speed of sound will be termed as "Mach-matched." While one can similarly do this to match Reynolds number by artificially prescribing the dynamic viscosity, the airfoil tables used for these simulations were generated for a fixed density of $\rho = 0.01$ kg/m^3 and dynamic viscosity of $\mu = 1.46 \times 10^{-5}$ N s/m^2. As a result, while important, effects from varying Reynolds numbers on airfoil performance will not be the focus of the analysis in this current paper.

Predicting Full-scale Dynamics

While the sub-scale vehicle is dynamically similar to the full-scale vehicle, the sub-scale vehicle is not dimensionally similar to the full-scale vehicle, meaning that a direct comparison of frequency responses may be misleading. For example, given the nature of the length ratios, the frequency at which modes occur do not inherently align. As a result, the dynamics are "scaled up" to the full-scale vehicle to compare the predicted dimensional stability and control derivatives, which are relevant for full-scale Chopper control design. In the context of this paper, this will be referred to as "inverse-scaling," and requires multiplying each derivative in the linear models by the appropriate factor. The scale-up factor for each derivative is the inverse of the corresponding scale-down method featured in Table 1 and is shown in Table 2 for each derivative in the reduced order model. Note that the density scaling does

not show up since the mass terms are separate in this representation. The same dimensional analysis methodology can be extrapolated to scale-up the full order linear stability and derivatives.

Table 2. Scale Up Factors for Dimensional Derivatives.

Derivative	Dimensions	Scale Up Factor
X_u, X_v, X_w Y_u, Y_v, Y_w Z_u, Z_v, Z_w L_p, L_q, L_r M_p, M_q, M_r N_p, N_q, N_r	$\frac{1}{T}$	$\frac{1}{\sqrt{N}}\sqrt{\frac{g_f}{g_s}}$
X_p, X_q, X_r Y_p, Y_q, Y_r Z_p, Z_q, Z_r	$\frac{L}{T}$	$\sqrt{N}\sqrt{\frac{g_f}{g_s}}$
$X_{\delta_q}, X_{\delta_p}, X_{\delta_w}, X_{\delta_r}$ $Y_{\delta_q}, Y_{\delta_p}, Y_{\delta_w}, Y_{\delta_r}$ $Z_{\delta_q}, Z_{\delta_p}, Z_{\delta_w}, Z_{\delta_r}$	$\frac{L}{T^2}$	$\frac{g_f}{g_s}$
L_u, L_v, L_w M_u, M_v, M_w N_u, N_v, N_w	$\frac{1}{LT}$	$\frac{1}{N\sqrt{N}}\sqrt{\frac{g_f}{g_s}}$
L_ϕ, L_θ, L_ψ M_ϕ, M_θ, M_ψ N_ϕ, N_θ, N_ψ $L_{\delta_q}, L_{\delta_p}, L_{\delta_w}, L_{\delta_r}$ $M_{\delta_q}, M_{\delta_p}, M_{\delta_w}, M_{\delta_r}$ $N_{\delta_q}, N_{\delta_p}, N_{\delta_w}, N_{\delta_r}$	$\frac{1}{T^2}$	$\frac{1}{N}\frac{g_f}{g_s}$

RESULTS

To validate the feasibility of the scaling methodology, sub-scale vehicles are evaluated in their ability to predict full-scale Chopper dynamics under progressively less constraining assumptions. First, length scales are varied at the same Martian environmental conditions (atmospheric density and gravity). Next, sub-scale vehicles are compared at the same density but different gravity and length scales. Finally, sub-scale vehicles of simultaneously varying lengths, gravity, and atmospheric density are compared, cumulating in a test matrix of 72 different sub-scale vehicle scenarios. A preliminary approach is then taken to downselect potential candidates for sub-scale testing based on various feasibility criteria.

Varying Length, Fixed Density and Gravity

Seven sub-scale vehicles of different length scales were modeled in reference to the Chopper full-scale vehicle in FLIGHTLAB for $\rho = 0.012$ kg/m^3 and $g = 3.71$ m/s^2. Table 3 outlines key nondimensional terms and modeling parameters, where the percentage indicates the sub-scale length relative to the full-scale vehicle. Across all vehicles, the Froude and Lock number, solidity, and blade loading are kept constant. Notably, both the Mach number and Reynolds number vary substantially with the relative vehicle length scale, despite increasing higher rotor speeds at smaller sub-scale sizes. The advancing tip Mach number disparity between the full-scale and sub-scale vehicles also grows as the advance ratio increases. While not included in the table, other parameters such as the vehicle inertias, blade mass distribution, flap hinge stiffness were also scaled accordingly, based on the methodology outlined in Table 1.

All vehicles were trimmed and linearized at hover and advance ratios of 0.056, 0.111, and 0.165 (equivalent to full-scale forward flight speeds of 10, 20, and 30 m/s, respectively), with and without Mach number matching. Fig. 3 shows the bare-airframe pitch response from 0.01 to 150 Hz for three sub-scale vehicles in hover without inverse scaling to full Chopper dimensions or Mach-matching. Decreasing the length-scale, and hence increasing the rotor speed from Froude-scaling, pushes the phugoid and blade flapping modes to higher frequencies but the same per/rev (for example, the flap mode occurs at roughly 1.3/rev for all vehicles).

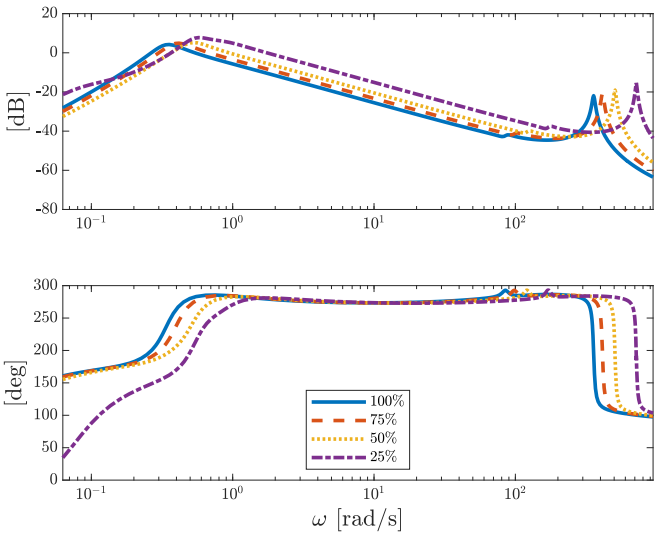

Figure 3. Full order q/δ_q frequency response for $\mu = 0$ without inverse-scaling or Mach-matching.

Fig. 4 shows the same frequency response inverse-scaled to the full-scale vehicle for a pitch on-axis response in hover, yet without Mach-matching. By applying the inverse scaling laws, the sub-scale vehicles better predict the phugoid and flap frequencies of the full-scale vehicle accurately. From here on, all figures will be shown to be inverse-scaled up for direct comparison to the full-scale vehicle dynamics. However, the smaller sub-scale vehicles, notably the 25% sub-scale vehicle, seem slightly less damped in the magnitude around the phugoid mode. This damping is primarily a result of the difference in Mach effects, as the rotors for the sub-scale vehicles operate at a lower Mach number compared to the full vehicle (0.39 Mach for the 25% vs. 0.77 Mach for the full-scale vehicle). The mitigation of Mach effects is shown in Fig. 5, where the tip Mach numbers were matched by artificially scaling the speed of sound, and the attenuation disappears for the

Table 3. Parameters of Sub-scale Vehicles vs. N at $\rho = 0.012$ kg/m^3 and $g = 3.71$ m/s^2.

	100%	87.5%	75%	62.5%	50%	37.5%	25%	12.5%
N	1	8/7	4/3	8/5	2	8/3	4	8
R [m]	0.675	0.59	0.51	0.42	0.34	0.25	0.17	0.08
Tip-to-Tip Distance [m]	3.43	3.00	2.57	2.14	1.71	1.29	0.86	0.43
Total Mass [kg]	33.0	22.1	13.9	8.1	4.13	1.74	0.52	0.06
RPM	2540	2715	2932	3212	3591	4147	5079	7183
γ	0.98	0.98	0.98	0.98	0.98	0.98	0.98	0.98
Hover, $\mu_x = 0$								
Fr	12868	12868	12868	12868	12868	12868	12868	12868
$\frac{C_T}{\sigma}$	0.126	0.126	0.126	0.126	0.126	0.126	0.126	0.126
M_{tip} (Not Ma-matched)	0.77	0.72	0.67	0.61	0.55	0.47	0.39	0.27
M_{tip} (Ma-matched)	0.77	0.77	0.77	0.77	0.77	0.77	0.77	0.77
$Re_{0.75}$	12300	10100	8000	6100	4400	2800	1500	500
$\mu_x = 0.111$								
V_∞ [m/s]	20.0	18.7	17.3	15.8	14.1	12.2	10.0	7.07
Fr	15895	15895	15895	15895	15895	15895	15895	15895
$\frac{C_T}{\sigma}$	0.1	0.1	0.1	0.1	0.1	0.1	0.1	0.1
M_{tip} (Not Ma-matched)	0.86	0.80	0.74	0.68	0.60	0.52	0.43	0.30
M_{tip} (Ma-matched)	0.86	0.86	0.86	0.86	0.86	0.86	0.86	0.86
$Re_{0.75}$	14200	11600	9200	7000	5000	3300	1800	630

predicted frequency responses. The full order frequency responses show fantastic alignment after being Mach-matched, validating the scaling process.

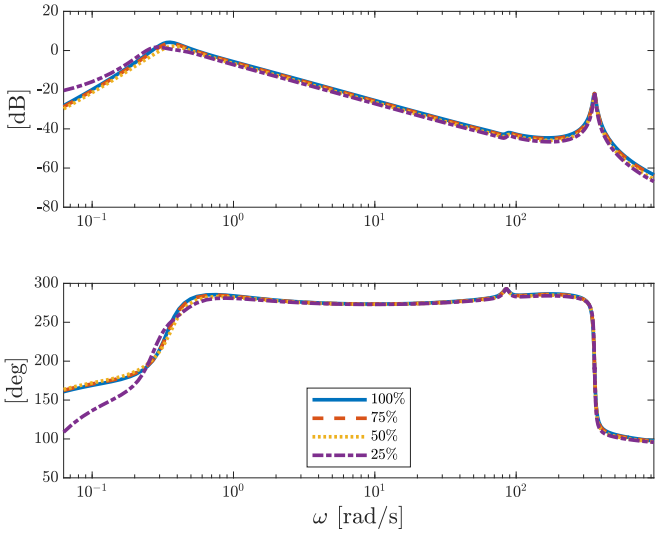

Figure 4. Full order q/δ_q frequency response for $\mu = 0$ with inverse-scaling but without Mach-matching.

The attenuation (and amplification) from Mach effects can be seen in Fig. 6, which enlarges the longitudinal phugoid mode for a 50% sub-scale vehicle in Mars density, showing the impact as a function of the severity of Mach number deviation. The red line indicates the full-scale Chopper linear model ($M_{tip} = 0.77$) and grayscale lines are for the 50% sub-scale's predicted full-scale linear model at varying degrees of Mach-matching. The dotted lines correspond to exceedances

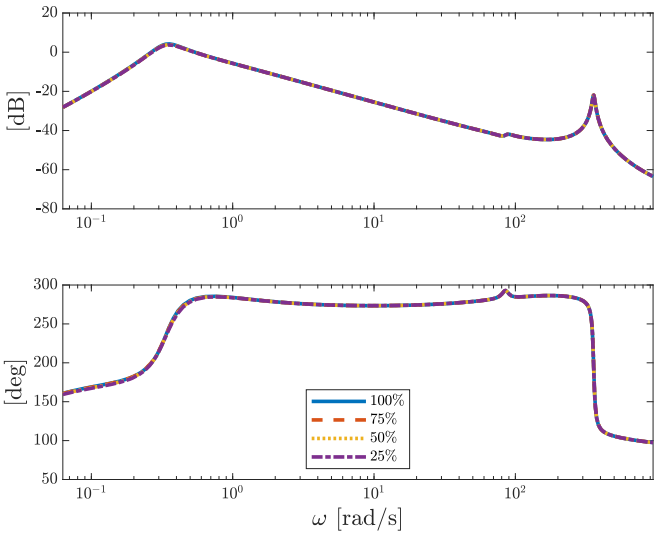

Figure 5. Full order q/δ_q frequency response for $\mu = 0$ with inverse-scaling and Mach-matching.

in the full-scale Chopper Mach number in hover ($M_{tip} > 0.77$) while the dashed lines correspond to hover tip Mach numbers lower than 0.77. From the figure, it can be seen that the lower the sub-scale tip Mach number, the more attenuated the gain of the longitudinal phugoid mode will be, matching the previous results seen in Fig. 4. More specifically, the 80% Mach-matched line corresponds to an overprediction in gain margin of about 9%, or around 0.28dB. Conversely, larger exceedances in sub-scale tip Mach amplify the magnitude of the mode, where a 20% overshoot causes an overprediction in gain margin by around 1.4%, or 0.09dB. Note that this may be valid in subsonic conditions and that substantive ex-

ceedances in the tip Mach number increasingly creep into the high sub-sonic regime (especially for forward flight) may invalidate such behavior.

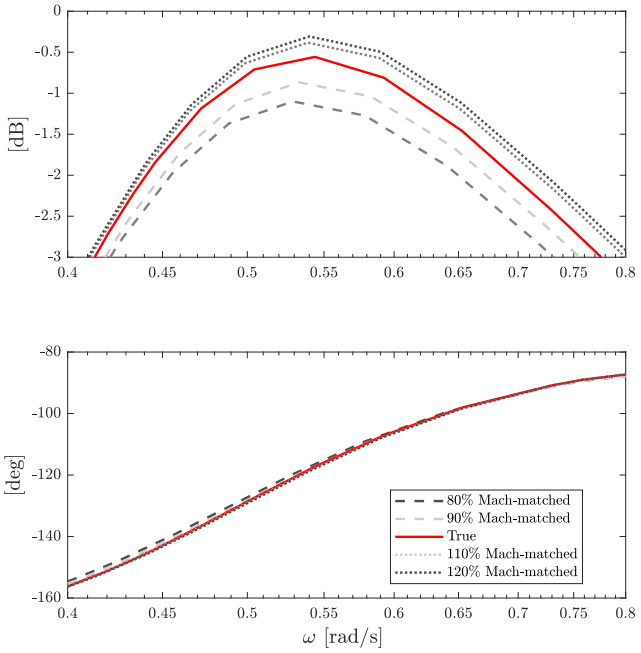

Figure 6. Magnitude variation of phugoid mode for q/δ_q at $\mu = 0$ from Mach effects. % indicates how close the sub-scale tip Mach number is relative to the full-scale Chopper tip Mach for the same condition.

The predicted reduced order open loop gain margins corroborate the impact of Mach-matching, as seen in Fig. 7. In hover, the difference in the average predicted gain margin from the Mach-matched runs provided more accurate results compared to the non-Mach-matched runs (5% off the full-scale pitch response gain margin compared to 20%). For all advance ratios except $\mu = 0.056$, Mach-matching results in less dispersion in the predicted gain margins. Furthermore, the sub-scale predicted margins underestimate the margin at higher speeds and overestimate in hover.

As aforementioned, the pitch-heave instability that arises in forward flight is of primary concern. To examine the forward flight characteristics of the sub-scale predicted linear models, Fig. 8 presents a root-locus of four vehicles at four different advance ratios without Mach-matching, focusing primarily on the evolution of the longitudinal and lateral phugoid modes. The colors indicate the sub-scale vehicle used to predict the full-scale behavior, and the poles of all four advance ratios are co-plotted. Both the Mach and non-Mach-matched cases reveal the same trend of an increasingly unstable mode caused by the growing angle of attack derivative. Furthermore, the smaller the sub-scale vehicle used to predict the full-scale, the more damped each pole is. When Mach effects are corrected, as seen in Fig. 9, the predicted full-scale poles align very closely with the full-scale Chopper poles. The remaining discrepancies are likely attributed to numerical differences in the simulation process.

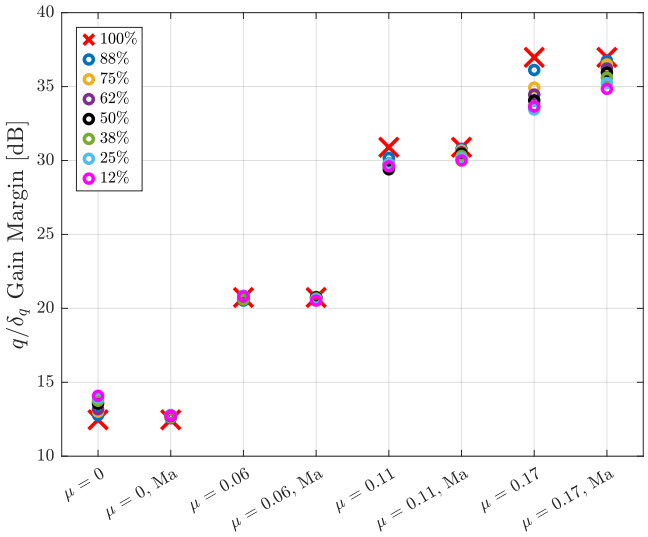

Figure 7. Reduced order longitudinal open loop gain margin vs. forward flight speeds and Mach-matching.

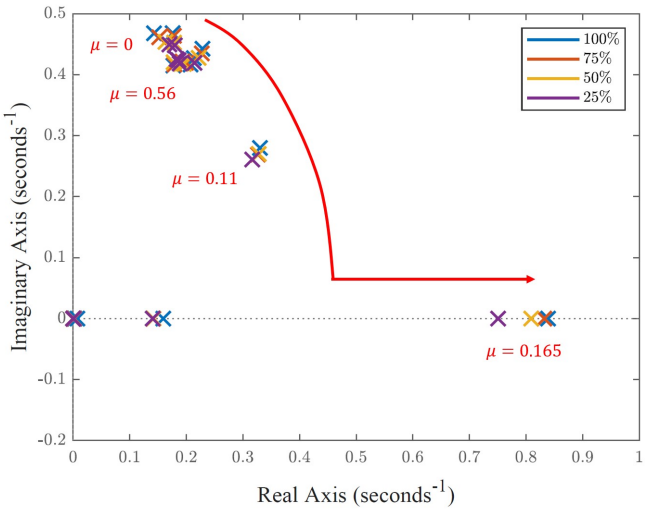

Figure 8. Growing forward flight instability due to increasing M_w for three predicted sub-scales without Mach-matching.

The Mach-matched plot of predicted M_w derivatives is shown in Fig. 10 as a function of the N length scale. The x-axis delineates the size of the sub-scale vehicle used to predict the derivative, and the line styles represent the various forward flight speeds. The red curves indicate the Mach-matched values and the light blue curves indicate the non-Mach-matched values. To determine if M_w can successfully be predicted from any sub-scale length, a dotted horizontal line at the value of the full-scale (100%) Chopper's M_w derivative is drawn. As a result, close adherence to the dotted line across sub-scale sizes shows up as a horizontal line at the value of the dotted 100% Chopper line. While the non-Mach-matched M_w predicts relatively well for lower advance ratios, there is a growing deviation as the forward flight speed increases and the length scale decreases (25% difference for a 12.5% vehicle at $\mu = 0.165$). Since the difference in Mach numbers for the smallest length scales is nontrivial (0.3 versus 0.9 for the

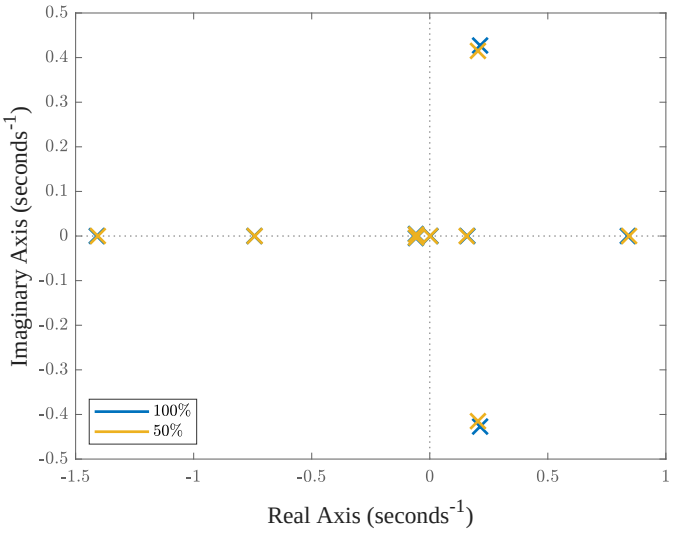

Figure 9. Pole-zero prediction from a 50% sub-scale for $\mu = 0.165$ with Mach-matching.

same conditions), these deviations are remedied when Mach effects are corrected, as seen by the approximately flat red line for the Mach-matched case.

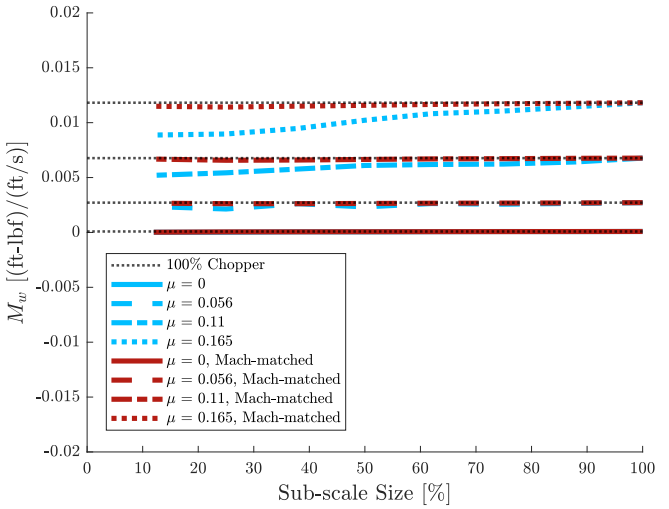

Figure 10. M_w from sub-scales vehicles of different lengths at $\rho = 0.012$ kg/m^3.

In conclusion, the full-scale linear dynamics can be predicted from sub-scale vehicles of varying lengths in Mars gravity and atmospheric density, especially for hover and lower advance ratios. Smaller sub-scale vehicles do bring poles closer to the origin and attenuate the full order longitudinal frequency response compared to the full-scale vehicle. While results for only the longitudinal axes is shown, other axes show similar results. Similarly, while M_w was predicted well, the pitch damping derivative M_u, was predicted with less accuracy. However, this did not significantly impact the predicted full-scale frequency response and gain margin, as seen by the alignment. Furthermore, as advance ratios increase, the difference in Mach number between the smallest scale vehicles and the full-scale Chopper grows, leading to increasing underpredictions of the gain margin in the longitudinal axis, and underpredictions of the angle of attack instability derivative. These differences are primarily due to Mach effects, and can be corrected once the tip Mach number is matched. As a result, by testing a sub-scale vehicle at the same gravity and atmospheric density (e.g. building a sub-scale to test in a sufficiently large vacuum chamber with a responsive gravity offload system), one could theoretically predict the full-scale dynamic behavior, capturing key dynamics in hover and forward flight.

Varying Length and Gravity, Fixed Density

However, vacuum testing is often expensive, time-constraining, and limited in availability. Therefore, it is of interest to examine if the dynamics of Mars rotorcraft can be predicted from simplified testing environments without the need for a gravity offload system. To that end, sub-scale models in Mars density but Earth gravity ($g = 9.81$ m/s^2) were simulated, and key parameters for four sub-scale vehicles are highlighted in Table 4. Since Froude number is a function of gravity, rotor speeds and forward flight speeds increase by a factor of $\sqrt{\frac{g_e}{g_m}} \approx 1.6$ for sub-scale vehicles when simulating from Earth gravity. Critically, despite Earth's higher speed of sound at 1atm, the tip Mach number also increases by approximately $\sqrt{\frac{g_e}{g_m}}\frac{a_m}{a_e} \approx 11\%$ for each trim scenario. Changing RPM also affects flap frequency, requiring scaling of the flap hinge stiffness if matching the flap response of the vehicle is desired. However, length scales, mass, Froude number, Lock number, and blade loading all remain the same as the prior Mars gravity case.

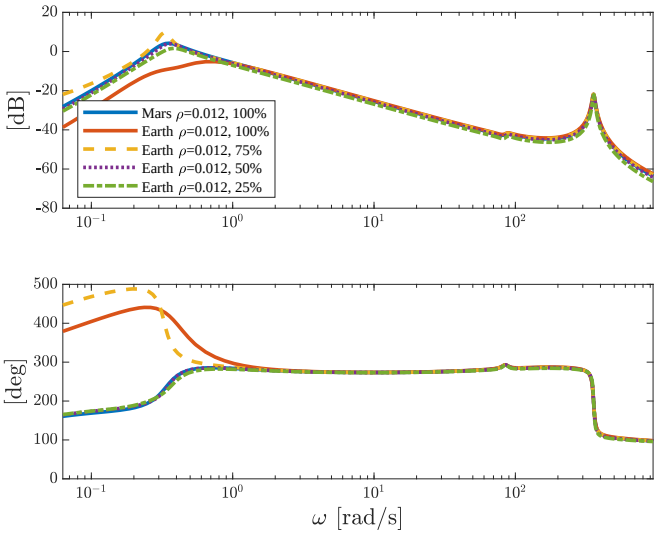

Figure 11. Full order q/δ_q frequency response for $\mu = 0$ with inverse-scaling but without Mach-matching for sub-scales in Earth and Mars gravity.

The full order pitch response in hover between inverse-scaled sub-scale vehicles in Earth gravity and Mars density ($\rho = 0.012$ kg/m^3) without Mach-matching and the full-scale

Table 4. Parameters of Sub-scale Vehicles vs. N at $\rho = 0.012\,\mathrm{kg/m^3}$ and Earth gravity.

	Mars 100%	Earth 100%	Earth 75%	Earth 50%	Earth 25%
Total Mass [kg]	33.0	33.0	13.9	4.13	0.52
RPM	2540	4129	4768	5839	8258
γ	0.98	0.98	0.98	0.98	0.98
Hover, $\mu_x = 0$					
Fr	12868	12868	12868	12868	12868
$\frac{C_T}{\sigma}$	0.126	0.126	0.126	0.126	0.126
M_{tip} (Not Ma-matched)	0.77	0.94	0.82	0.67	0.47
$Re_{0.75}$	12300	18800	12200	6600	2300
$\mu_x = 0.111$					
V_∞ [m/s]	20.0	32.5	28.2	23.0	16.3
Fr	15895	15895	15895	15895	15895
$\frac{C_T}{\sigma}$	0.1	0.1	0.1	0.1	0.1
M_{tip} (Not Ma-matched)	0.86	1.05	0.91	0.74	0.52
$Re_{0.75}$	14200	21600	14000	7600	2700

Chopper is shown in Fig. 11. Note that the flap frequency has been matched by scaling the blade bending stiffness, modeled by scaling the hinge stiffness. Aside from variations in the magnitude of the frequency regime below 1 rad/s, the general response across all sub-scale lengths is very similar. As in the Mars gravity case, the amplitude of the lower frequency response is susceptible to Mach effects, where sub-scale vehicles with tip Mach numbers greater than the full-scale vehicle overshoot the gain and ones with lower tip Mach numbers are more attenuated, with the exception of the 100% Earth gravity vehicle. This sub-scale vehicle has a high sub-sonic tip Mach of 0.94 in hover, which resulted in a severely attenuated phugoid response. These variations in magnitude are corrected in the Mach-matched case, shown in Fig. 12.

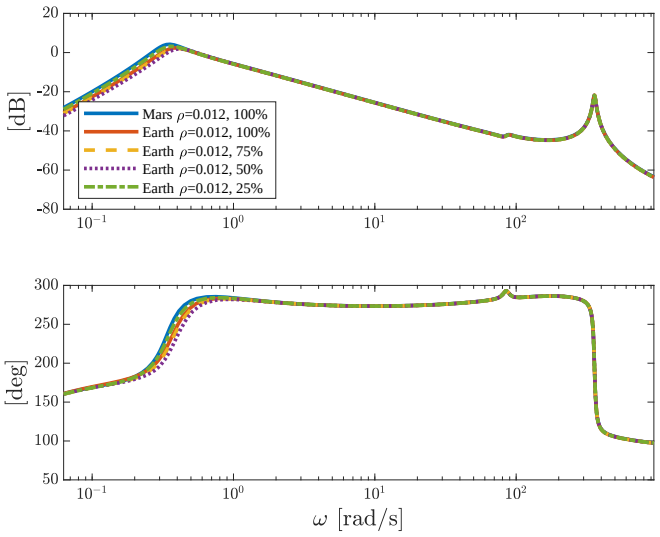

Figure 12. Full order q/δ_q frequency response for $\mu = 0$ with inverse-scaling and Mach-matching for sub-scales in Earth and Mars gravity.

Complications arise when comparing in forward flight. At higher forward flight speeds, the frequency of vehicle and rotor modes are captured from the various sub-scales, but the magnitude is not fully captured even when Mach effects are corrected, as seen in Fig. 13. The lower frequency deviations are potentially attributable to numerical discrepancies in the inverse-scaling of the inflow states which are removed in the model reduction. This can be seen in Fig. 14, as the reduced order pitch response in forward flight shows significantly better adherence, even without Mach-matching.

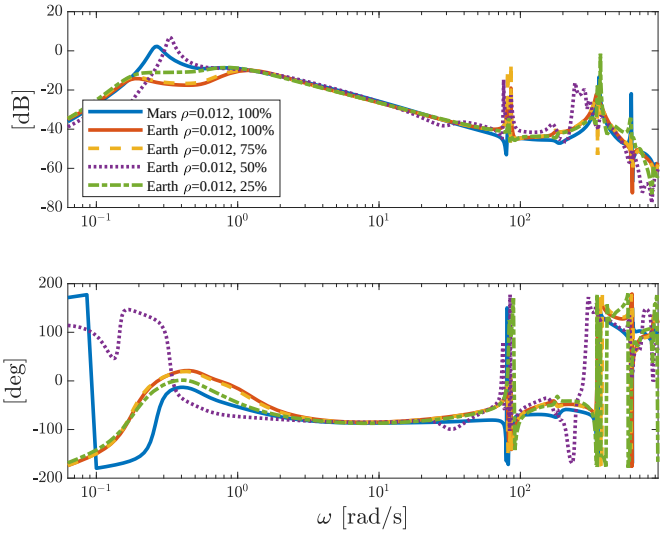

Figure 13. Full order q/δ_q frequency response for $\mu = 0.11$ with inverse-scaling and Mach-matching for sub-scales in Earth and Mars gravity.

The reduced order gain margin for different advance ratios with and without Mach-matching is shown in Fig. 15. In hover, the Earth gravity sub-scale models without Mach-matching generally overpredict by 0.8dB on average, where decreasing sub-scale size correlates to larger overpredictions.

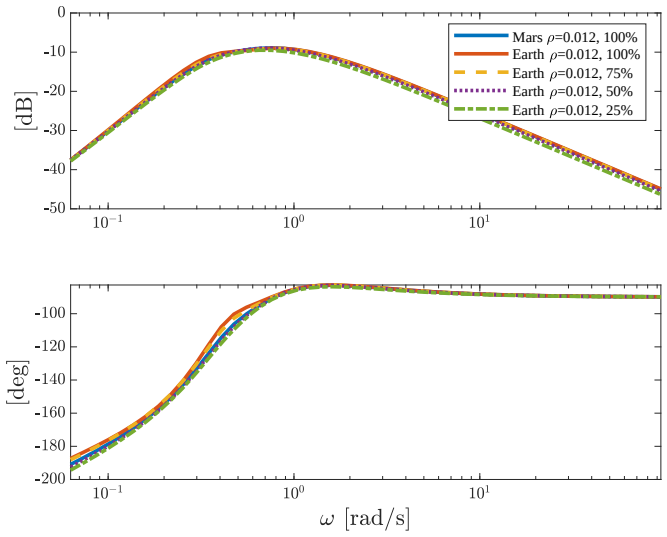

Figure 14. Reduced order q/δ_q frequency response for $\mu = 0.11$ with inverse-scaling but without Mach-matching between Earth and Mars gravity sub-scales.

The trend reverses for advance ratios of 0.11 and 0.165, where the smaller sub-scales tend to underpredict the gain margin the most, and larger sub-scales overpredict. There is improvement in gain margin prediction when Mach-matching, especially for the hover and $\mu = 0.165$ cases.

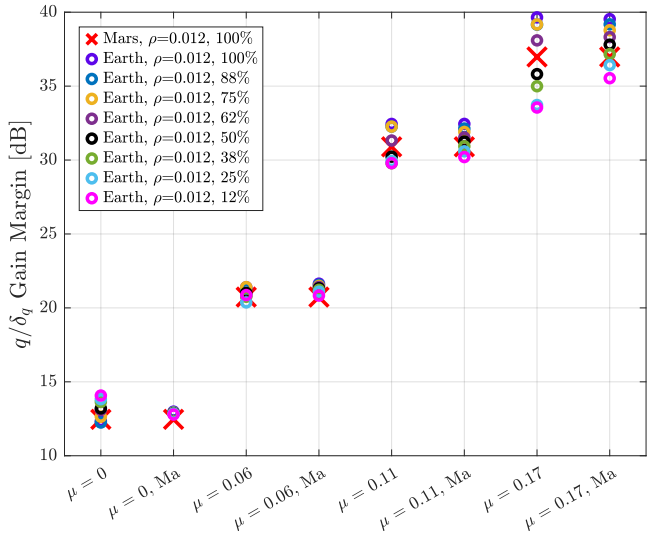

Figure 15. Reduced order longitudinal open loop gain margin vs. advance ratio and Mach-matching.

To conclude the low atmospheric density, Earth gravity analysis, the Mach-matched inverse-scaled angle of attack derivative, M_w, is shown in Fig. 16. While in ideal environmental conditions, this figure predicts that even with a different gravity, this derivative can be estimated given any size sub-scale vehicle. The real-world analog would entail Earth testing in either a vacuum chamber without a gravity offload system or outside at a sufficiently high altitude. The results show that while the discrepancies in gain margin and full order frequency response are larger at higher forward flight speeds for the Earth gravity case, the methodology remains consistent, especially for reduced order model estimation.

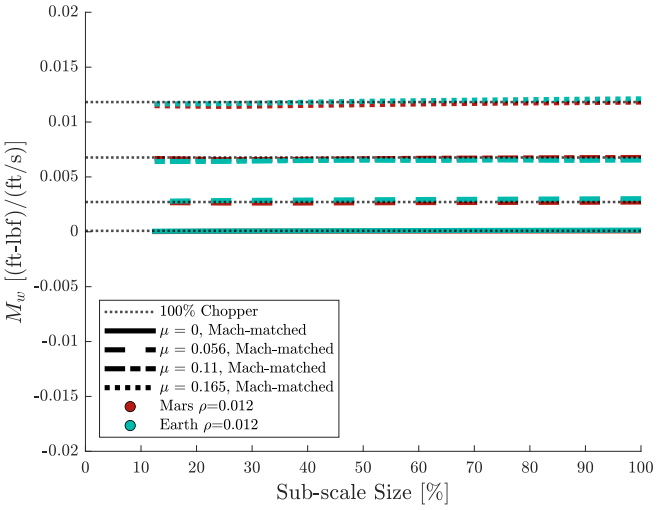

Figure 16. M_w from sub-scale vehicles of different lengths and gravitational accelerations at $\rho = 0.012$ kg/m^3.

Varying Length, Gravity, and Density

Full Earth to Mars scaling requires varying density, in addition to gravity, and length-scales. While density variations do not directly impact Froude number, they do impact the thrust coefficient, C_T, which consequently affects mass, inertia, and flap hinge stiffness/damping scaling. Nine densities, ranging from $\rho = 0.012$ to 1.225 kg/m^3, in addition to the eight length-scales, were selected to create sub-scale vehicles that were trimmed and linearized in Earth gravity ($g = 9.81$ m/s^2). All were simulated with and without Mach-matching, as well as at the 4 advance ratios, resulting in over 500 unique scaled linear models. To simplify comparisons, the "mass ratio," defined as $\frac{m_s}{m_f} = \frac{1}{N^3}\frac{\rho_s}{\rho_f}$, is used as a comparative heuristic since it is a function of both the atmospheric density and length scale. Intuitively, it relates the sub-scale mass to the mass of the full-scale Chopper. Table 5 outlines the key non-dimensional parameters for a few sub-scale vehicles of the same size at varying densities. The blade loading, Lock number, Froude number, and advance ratios remain matched. Notably, the Reynolds number grows dramatically as the density increases.

The full-scale Chopper's longitudinal frequency response in hover remained very well predicted across density variations even without Mach-matching. Fig. 17 highlights the difference in predicted full-scale longitudinal gain margin for the reduced order linear model in hover. For simulations that were not Mach-matched, larger sub-scale vehicles ($\geq 87.5\%$) predicted the margins within 2% of the full-scale at all densities other than $\rho = 1.225$ kg/m^3. As the sub-scale size decreases, the predicted gain margin is increasingly overestimated, as seen in both previous Mars and Earth gravity cases. Conversely, the Mach-matched cases provided consistent gain margin overpredictions $\approx 3-5\%$ for the vast majority of sub-scale size and density combinations. The highest atmospheric

Table 5. Parameters of Sub-scale Vehicles vs. N at Varying Densities and Earth gravity.

	Mars	Earth	Earth	Earth	Earth	Earth
	100%	75%	75%	75%	75%	75%
ρ [kg/m^3]	0.012	0.012	0.358	0.531	0.878	1.225
Mass Ratio	1.0	0.42	12.6	18.7	30.9	43.1
RPM	2540	4768	4768	4768	4768	4768
γ	0.98	0.98	0.98	0.98	0.98	0.98
Hover, $\mu_x = 0$						
Fr	12868	12868	12868	12868	12868	12868
$\frac{C_T}{\sigma}$	0.126	0.126	0.126	0.126	0.126	0.126
M_{tip} (Not Ma-matched)	0.77	0.82	0.86	0.82	0.77	0.74
$Re_{0.75}$	12300	12200	394600	545100	818500	1070000
$\mu_x = 0.111$						
V_∞ [m/s]	20.0	28.2	28.2	28.2	28.2	28.2
Fr	15895	15895	15895	15895	15895	15895
$\frac{\bar{C}_T}{\sigma}$	0.1	0.1	0.1	0.1	0.1	0.1
M_{tip} (Not Ma-matched)	0.86	0.91	0.95	0.91	0.86	0.83
$Re_{0.75}$	14200	14000	454400	627600	942400	1232000

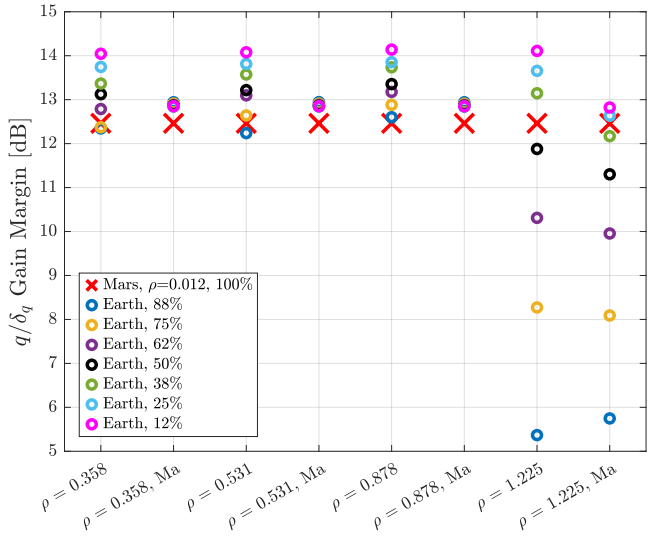

Figure 17. Reduced order longitudinal open loop gain margin in hover for various atmospheric densities, with and without Mach-matching.

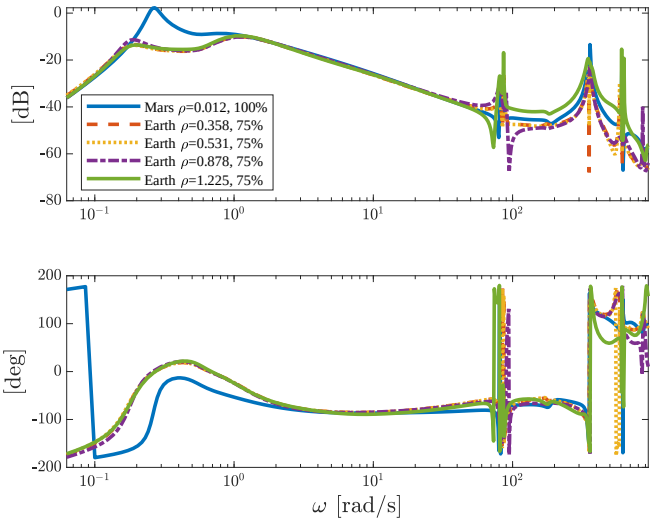

Figure 18. Full order q/δ_q frequency response for $\mu = 0.11$ with inverse-scaling and Mach-matching between Earth and Mars gravity sub-scales in various air densities.

density case shows the largest dispersion in predicted gain margin, where the largest sub-scale vehicles have errors exceeding 20%, of which the causes are not entirely resolved at this time. These deviations are similarly seen in the Mach-matched case. Similar trends can be found for the gain margin tables for the forward flight cases, except the deviation in gain margin at the smallest sub-scales is lower (around 9% for $\mu = 0.165$) and the differences at the largest sub-scales are slightly higher ($\approx 7-8\%$).

A comparison of the predicted full-scale Chopper longitudinal response from 75%-length sub-scales at $\mu = 0.11$ is shown in Fig. 18. The general location of the various higher order modes align, as expected from scaling the rotor blade stiffness. The phugoid mode is especially more damped for the Earth conditions compared to the Mars case and matches the same behavior as the 75% sub-scale in the Earth $\rho = 0.012$ kg/m^3 case in Fig. 13. Without Mach-matching, the frequency response (not pictured) reveals worse adherence in the lower frequencies and greater variability in the higher frequency (> 100 rad/s) regime. These are predominantly from higher order terms such as the flapping and inflow, as seen in the better adherence in the non-Mach-matched reduced order response, shown in Fig. 19.

Similarly, predicting the poles at different forward flight speeds continues to match across various Earth atmospheric densities as seen in Fig. 20. As seen previously, the longitudinal phugoid mode continues to track the full-scale evolution with respect to higher forward flight speeds. However, there is also a general trend that the Earth densities slightly underpredict the magnitude of the instability of the poles, but this

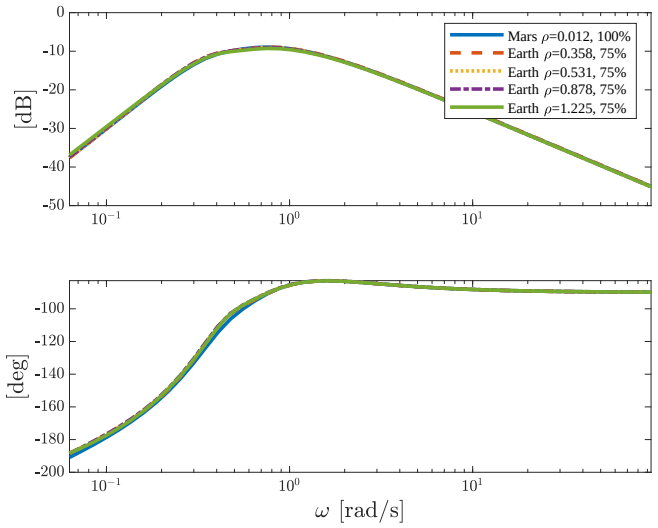

Figure 19. Reduced order q/δ_q frequency response for $\mu = 0.11$ with inverse-scaling but without Mach-matching between Earth and Mars gravity sub-scales in various air densities.

is remedied once Mach effects are matched as seen in Fig. 21. Furthermore, for larger sub-scales at higher atmospheric densities, there is a consistent exaggeration of the instability of the poles, overpredicting the magnitude slightly at the highest densities. Conversely, the smaller sub-scale vehicles provide a more consistent prediction with the poles.

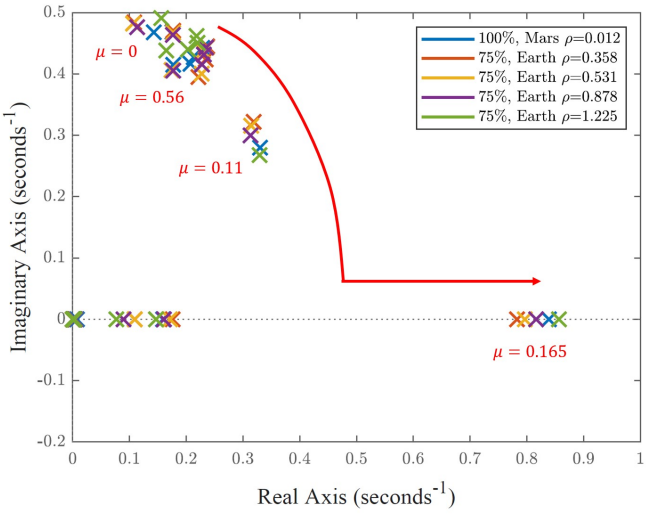

Figure 20. Growing forward flight instability due to increasing M_w for a 75% sub-scale vehicle in various air densities without Mach-matching.

As a result, it remains critical to see if the angle of attack stability derivative (M_w) can be estimated from Earth conditions. Fig. 22 and Fig. 23 show the predicted M_w derivative from all environments and length-scales for all forward flight speeds without and with Mach-matching, respectively. Derivatives are plotted against a logarithmic vehicle mass ratio, where mass ratios $\gg 1$ indicate a substantively larger sub-scale mass relative to the full-scale Chopper. Similar to the

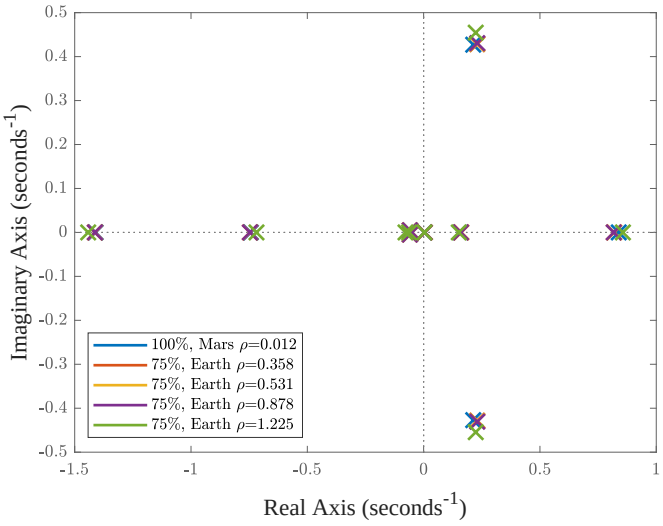

Figure 21. Pole-zero prediction from a 75% sub-scale for $\mu = 0.165$ in various air densities with Mach-matching.

Earth $\rho = 0.012\,\mathrm{kg/m^3}$ case, there is an increasing underprediction of the derivative as the advance ratio increases, indicated by a growing deviation from the full-scale Chopper's values. This deviation widens as the mass ratio decreases, indicating similar trends to the previous cases where smaller sub-scales underpredicted the derivative value.

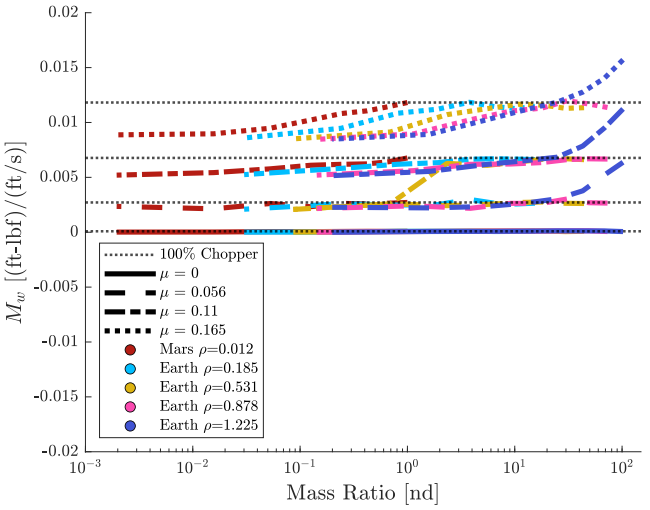

Figure 22. M_w from sub-scale vehicles of different lengths, gravitational accelerations, and atmospheric densities without Mach-matching.

Most of these effects are remedied when looking at the Mach-matched equivalents, where M_w predictions are consistent across the vast majority of mass-ratios. However, the largest vehicles in the Earth $\rho = 1.225\,\mathrm{kg/m^3}$ (75%, 88%, and 100%-size sub-scales) continue to depict a substantive deviation in the full-scale prediction, similar to the gain margin analysis. This is found in both the non-Mach-matched and Mach-matched cases and is an area for further investigation.

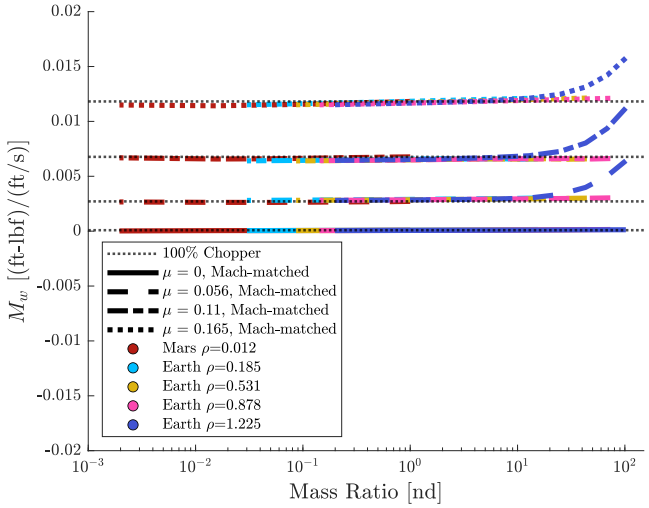

Figure 23. M_w from sub-scale vehicles of different lengths, gravitational accelerations, and atmospheric densities with Mach-matching.

In conclusion, the scaling methodology continues to predict key longitudinal dynamics characteristics of the full-scale vehicle even in varying atmospheric density. Mach-matching does provide slight improvements, especially in predicting full-scale gain margins from smaller length scale vehicles. Similarly, vehicles that were operating close to the desired Mach number (e.g. the 75% sub-scale at $\rho = 0.878$ kg/m^3) also predicted values that were closer to the full-scale Chopper's. However, predictions from larger sub-scale sizes at the highest density ($\rho = 1.225$ kg/m^3) show significant decreases in predictive accuracy for both the longitudinal gain margin and the M_w derivative.

Limitations and Feasibility

While promising, the results shown rely on assumptions that may be infeasible in practice. For example, the mass estimation does not take into account the more granular scaling of individual subcomponents of the vehicle, such as the batteries and motors. Potential Reynolds effects were not examined, and the airfoil performance look-up tables were assumed to be the same at every atmospheric condition. This potentially overestimates the lift generation for the smaller sub-scale vehicles at lower densities and underestimates their efficiency at significantly higher densities. Stall and near-stall predictions are also assumed to be the same. Furthermore, part of the test matrix of length-scales and densities contains sub-scale vehicles that are, at the minimum, physically complex to manufacture, and more likely than not, practically infeasible.

Vehicle mass scales with $\frac{\rho_s}{\rho_f}\frac{1}{N^3}$, indicating that smaller length-scales decrease vehicle mass by N^3, while greater atmospheric densities linearly increase the total vehicle mass. As a result, sub-scale vehicles ranging from 0.06 (lowest density and smallest size) to $>$ 3000 kg (highest density and largest size) were included in the analysis. Fig. 24 shows a heatmap of the 72 sub-scale vehicles modeled, where each square is labeled with its respective mass. The rows denote the gravity and atmospheric density and the columns indicate the length of the sub-scale vehicle relative to the full-scale. The bottom right corner represents the full-scale Mars Chopper vehicle in condition. Darker regions of the heatmap indicate sub-scales with a similar mass to the full-scale vehicle. Outside of the highest density case, the larger sub-scale vehicles tended to best predict the longitudinal gain margin, especially since the tip Mach numbers remained closest to the full-scale vehicle's. However, many of these vehicles are high in mass, and practical considerations, such as ease of transport, favor vehicles that are smaller, especially at higher density atmospheric conditions. This may come at the expense of the integrity of the full-scale flight dynamics prediction, especially when Mach number is not scaled. Conversely, the smallest vehicles at lower densities have a significantly constrained mass budget that may struggle to accommodate heavier subcomponents. As a result, testing in $\rho = 1.225$ kg/m^3 and Earth gravity likely requires smaller (e.g. 12.5% or 25%) sub-scale vehicles while testing in $\rho = 0.012$ kg/m^3 offers more flexibility.

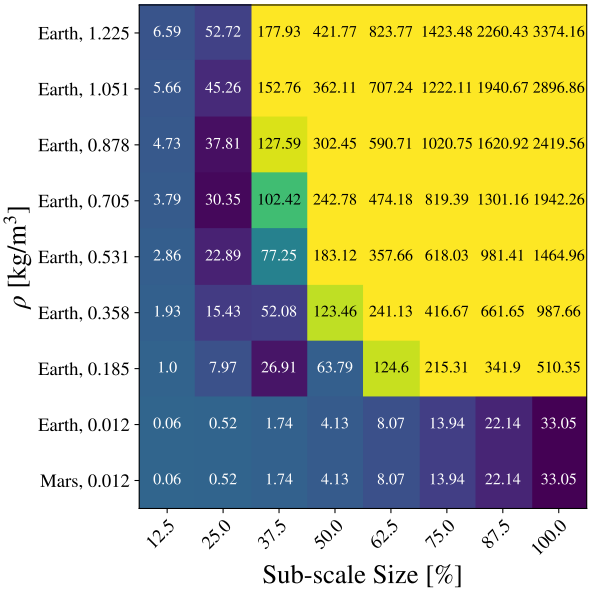

Figure 24. Matrix of feasible vehicle mass [kg].

Furthermore, while it is possible to match the flap frequency by scaling the hinge stiffness in simulation, matching the flap stiffness in practice is nontrivial, especially when simultaneously scaling the blade inertia, and hence mass distribution. This appears in the volumetric density of the blade (ρ_b), which is scaled by $\frac{g_f}{g_s}\frac{I_{b_f}}{I_{b_s}}N^5$ to match the blade flapping stiffness (EI_b). Fig. 25 provides a heatmap of the test configurations shown and the corresponding blade volumetric density needed. The tiles that have no values require blade densities that exceed the volumetric density of steel. If the intention is to maintain the blade density around $\rho_b = 0.0015$ g/mm^3, the material density for carbonfiber, only a few vehicles would provide likely options, including a 62.5% vehicle flown in $\rho = 0.531$ kg/m^3. Otherwise, scaling the corresponding stiffness for an Earth atmospheric density would potentially re-

quire blades to be made of higher densities such as aluminum and steel. Forgoing scaling of the blade flap response is a reasonable approach as long as the flap frequency remains sufficiently outside the bandwidth of control and simultaneously ensure that the Mars blades can structurally withstand the larger drag forces at greater air densities.

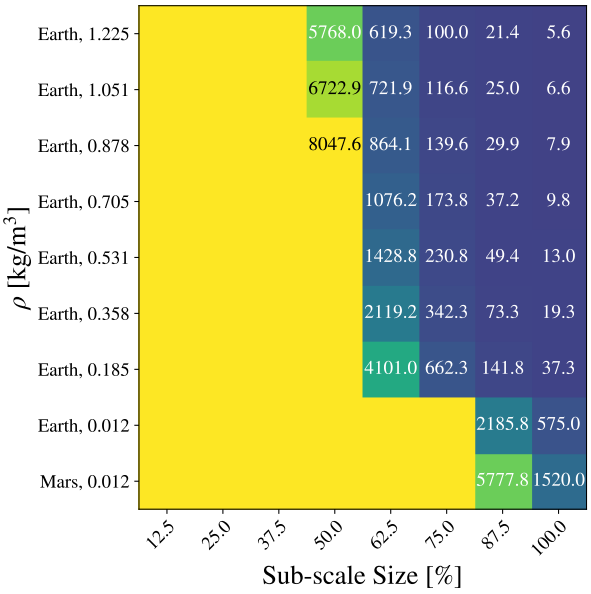

Figure 25. Matrix of feasible blade densities [kg/m^3].

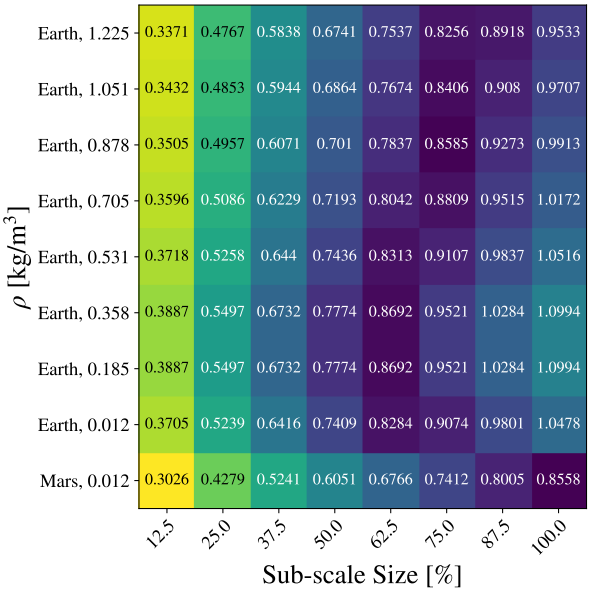

Figure 26. Matrix of feasible Mach numbers for $\mu = 0.11$.

Finally, results have shown that neglecting Mach effects may contribute to deviations in frequency response analysis, especially for smaller sub-scale vehicles when the difference in Mach numbers grows. Fig. 26 reveals a region of feasibility (demarcated in dark blue) in the test matrix that has the closest tip Mach number to the full-scale vehicle without the need for any Mach-matching at the highest advance ratio. Otherwise, matching Mach numbers would require manipulating the test environment's speed of sound, potentially by altering the gas composition of a testing chamber such as using refrigerant (Ref. 6) or flying at a sufficiently high altitude.

Cumulatively, designing a sub-scale vehicle that satisfies all three of the above conditions, in addition to the scaling laws, may be challenging. For example, a 62.5% sub-scale flying on Earth at a low atmospheric density of $\rho = 0.531$ kg/m^3 has a very similar tip Mach number and requires a similar blade density to Chopper, but also requires a vehicle mass 10 times the Chopper vehicle. As a result, it is likely that at least one of the physical parameters has to be sacrificed in order to arrive at a practical solution.

CONCLUSIONS

Sub-scale vehicles of varying sizes were developed using Froude scaling laws to evaluate their ability to predict full-scale dynamics of the next-generation Mars rotorcraft, Chopper. Blade loading, Lock number, and flap frequencies were also matched and scaling relationships derived. The methodology was tested to predict full-scale frequency response, gain margin, and stability characteristics in hover and forward flight for a matrix of Mars and Earth gravitational accelerations and atmospheric densities. Generally, smaller length-scale vehicles demonstrated slightly worse predictive capability primarily due to Mach effects, which could be corrected if the speed of sound was adjusted to match the advancing tip Mach number of the full-scale vehicle. Longitudinal effects such as the pitch-heave instability at higher forward flight speeds were also successfully replicated from all conditions, but were more correctly estimated if Mach effects were accounted for. Sub-scale vehicles at the highest density also suffered in predictive capability, leading to larger deviations in predicted values of the angle of attack stability derivative M_w and gain margins. Limitations in vehicle mass, blade density and material, and Mach-matching capabilities constrain feasibility for the full sub-scale matrix, and must be considered for implementation, potentially necessitating the sacrifice of one aspect of matching. However, if accounted for, it has been shown that given the right conditions, a sub-scale model of varying length in a different atmospheric density and gravity has the potential to predict the full-scale Chopper dynamics, at least in a reduced-order state space representation.

FUTURE WORK

This paper has confirmed that Froude scaling can be applied to create sub-scale vehicles that predict full-scale Mars rotorcraft linear flight dynamics in simulation. However, improvements can be made to the analysis. Using dedicated airfoils to properly account for Reynolds number effects for each sub-scale size and flight condition would provide more realistic rotor performance estimation, which might affect trim conditions and further inform which vehicles are more practically feasible. Furthermore, the inclusion of higher fidelity inflow modeling through FLIGHTLAB's VVPM and the inclusion of rotor-rotor interference would improve the accuracy

of the modeling (for example, the longitudinal speed damping derivative, X_u, is sensitive to longitudinal variations of the inflow). Finally, nonlinear response through system identification should be performed both in simulation and in experimentation to validate the findings. Low pressure testing facilities at NASA Ames and JPL may provide opportunities to perform sub-scale free flight system identification for comparison.

Author contact:

- Allen Ruan allen.w.ruan@nasa.gov
- Tove Ågren tove.s.aagren@nasa.gov

ACKNOWLEDGMENTS

This work was carried out under funding from the New Business Council at NASA Ames Research Center, which the authors thank for their resources and support. The authors would like to express their gratitude to Carlos Malpica, Wayne Johnson, David Caudle, Jeremy Aires, Witold Koning, Nicholas Peters, Carlos Pereyra, Gianmarco Sahragard-Monafred, and Sesi Kottapalli for their technical expertise and editorial feedback. Furthermore, the authors thank Lucas Rowden and Jett Wong-Parker, Rotorcraft Aeromechanics Summer 2024 interns, for their early contributions to the project. Finally, the authors would like to acknowledge the support of Shannah Withrow-Maser, Carl Russell, Dr. William Warmbrodt, and Larry Hogle during this research.

REFERENCES

1. Johnson, W., Withrow-Maser, S., Young, L., Malpica, C., Koning, W. J. F., Kuang, W., Fehler, M., Tuano, A., Chan, A., Datta, A., Chi, C., Lumba, R., Escobar, D., Balaram, J., Tzanetos, T., and Grip, H., "Mars Science Helicopter Conceptual Design," NASA TM 220485, 2020.

2. Grip, H. F., Jones-Wilson, L., Lefler, C., Duran, A., Inouye, B., Burns, B., Metz, B., Brown, T., Bugby, D., Karras, J., Mier-Hicks, F., Tzanetos, T., Picache, G., Johnson, W., Ueno, M., Sahragard-Monfared, G., and Bowman, J., "The CHOPPER Next-Generation Mars Rotorcraft: Scaling Ingenuity by a Factor 20," IEEE, Santa Clara, CA, February 2025.

3. Tischler, M. B., and Remple, R. K., *Aircraft and Rotorcraft System Identification*, American Institute of Aeronautics and Astronautics, Reston, VA, 2012. DOI: 10.2514/4.868207.

4. Grip, H. F., Johnson, W., Malpica, C., Scharf, D. P., Mandić, M., Young, L., Allan, B., Mettler, B., Martin, M. S., and Lam, J., "Modeling and Identification of Hover Flight Dynamics for NASA's Mars Helicopter," *Journal of Guidance, Control, and Dynamics*, Vol. 43, (2), 2020, pp. 179–194. DOI: 10.2514/1.G004228.

5. Aagren, T. S., Ruan, A. W., Malpica, C., Withrow-Maser, S., and Meyn, L., "In-flight System Identification of the Ingenuity Mars Helicopter," AIAA SciTech 2025 Forum, Orlando, FL, 2025.

6. Wolowicz, C. H., Bowman, J. S., and Gilbert, W. P., "Similitude Requirements and Scaling Relationships as Applied to Model Testing," NASA Technical Paper 1435, 1979.

7. Owens, B., Brandon, J., Croom, M., Fremaux, C. M., Heim, E., and Vicroy, D., "Overview of Dynamic Test Techniques for Flight Dynamics Research at NASA LaRC," AIAA 25th Aerodynamic Measurement Technology and Ground Testing Conference, San Francisco, CA, June 2006.

8. Chambers, J. R., *Modeling Flight: The Role of Dynamically Scaled Free-Flight Models in Support of NASA's Aerospace Programs*, Government Printing Office, 2009. DOI: NASA SP 2009-575.

9. Curtiss, H., Putman, W., and Martinez, E., "The Evaluation of Stability and Control Characteristics of Aircraft at Low Speeds Using Dynamically Similar Models in Semi-Free Flight," American Helicopter Society 18th Annual Forum, Washington, DC, May 1962.

10. Hunt, G. K., "Similarity Requirements for Aeroelastic Models or Helicopter Rotors," Royal Aircraft Establishment C.P. 1245, 1972.

11. Friedmann, P., "Aeroelastic Scaling For Rotary-Wing Aircraft with Applications," 42nd AIAA/ASME/ASCE/AHS/ASC Structures, Structural Dynamics, and Materials Conference, Reston, VA, April 2001.

12. Mettler, B., Tischler, M., and Kanade, T., "System Identification of Small-Size Unmanned Helicopter Dynamics," American Helicopter Society 55th Annual Forum, Montreal, Quebec, Canada, May 1999.

13. Mettler, B., Tischler, M., and Kanade, T., "System Identification Modeling of a Small-Scale Unmanned Rotorcraft for Control Design," *Journal of the American Helicopter Society*, Vol. 47, (1), 2002, pp. 50–63. DOI: 10.4050/JAHS.47.50.

14. Mettler, B., Dever, C., and Feron, E., "Scaling Effects and Dynamic Characteristics of Miniature Rotorcraft," *AIAA Journal of Guidance, Control, and Dynamics*, Vol. 27, (3), 2004, pp. 466–478. DOI: 10.2514/1.10336.

15. Ivler, C. M., Rowe, E. S., Martin, J., Lopez, M. J. S., and Tischler, M. B., "System Identification Guidance for Multirotor Aircraft: Dynamic Scaling and Test Techniques," *Journal of the American Helicopter Society*, Vol. 66, (2), April 2021, pp. 1–16. DOI: 10.4050/JAHS.66.022006.

16. Ivler, C. M., Goerzen, C. L., Wagster, J. A., Sanders, F. C., Cheung, K. K., and Tischler, M. B., "Control Design for Tracking of Scaled MTE Trajectories on an IRIS+ Quadcopter," American Helicopter Society 74th Annual Forum, Phoenix, AZ, May 2018.

17. Ivler, C., Truong, K., Kerwin, D., Otomize, J., Parmer, D., Tischler, M., and Gowans, N., "Development and Flight Validation of Proposed Unmanned Aerial System Handling Qualities Requirements," *Journal of the American Helicopter Society*, Vol. 67, (1), January 2022, pp. 1–18. DOI: 10.4050/JAHS.67.012002.

18. Singh, R., "Hexacopter Flight Dynamics on Earth and Martian Surfaces," Vertical Flight Society Sixth Decennial Aeromechanics Specialists' Conference, Santa Clara, CA, February 2024.

19. Withrow-Maser, S., Johnson, W., Koning, W., Ågren, T., Sahragard-Monfared, G., Bowman, J., Ruan, A., Kaweesa, D., and Malpica, C., "Critical Aerodynamic and Performance Upgrades to Enable Larger Mars Rotorcraft Such as the Chopper Platform," Vertical Flight Society 81st Annual Forum, Virginia Beach, VA, May 2025.

20. Ågren, T., Peters, N., and Ruan, A., "Rotor Wake Modeling for Mars Rotorcraft using the Viscous Vortex Particle Method," Vertical Flight Society 81st Annual Forum, Virginia Beach, VA, May 2025.

21. Sahragard-Monfared, G., Bowman, J., Koning, W., and Johnson, W., "Effects of Solidity, Number of Blades, and Chord Distribution on Rotor Performance in a Martian Environment," Vertical Flight Society 81st Annual Forum, Virginia Beach, VA, May 2025.

22. Du Val, R., and He, C., "FLIGHTLAB Modeling for Real-Time Simulation Applications," *International Journal of Modeling, Simulation, and Scientific Computing*, Vol. 08, (04), 2017, pp. 1743003. DOI: 10.1142/S1793962317430036.

23. Peters, D. A., and He, C. J., "Finite State Induced Flow Models Part II: Three Dimensional Rotor Disk," *Journal of the Aircraft*, Vol. 32, (2), 1995, pp. 323–333. DOI: 10.2514/3.46719.

24. Johnson, W., *Rotorcraft Aeromechanics*, Vol. 36, Cambridge University Press, 2013. DOI: 10.1017/CBO9781139235655.

25. Grip, H. F., Johnson, W., Malpica, C., Scharf, D. P., Mandic, M., Young, L., Allan, B., Mettler, B., and San Martin, M., "Flight Dynamics of a Mars Helicopter," 43rd European Rotorcraft Forum, Milan, Italy, 2017.

26. Sobron, A., Lundström, D., and Krus, P., "A Review of Current Research in Subscale Flight Testing and Analysis of Its Main Practical Challenges," *Aerospace*, Vol. 74, (8), 2021, pp. 323–333. DOI: 10.3390/aerospace8030074.

27. Alvarenga, J., Vitzilaios, N., Rutherford, M., and Valavanis, K., "Scaled Control Performance Benchmarks and Maneuvers for Small-Scale Unmanned Helicopters," 54th IEEE Conference on Decision and Control (CDC), Osaka, Japan, December 2015.